Debye-diffraction-based concentric energy analysis on two-photon photoluminescence imaging of gold nanorods under radial polarization illumination

Hong Kang and Min Gu[a)]
Centre for Micro-Photonics, Faculty of Engineering and Industrial Sciences, Swinburne University of Technology, Hawthorn, Victoria 3122, Australia

(Received 14 June 2012; accepted 25 September 2012; published online 22 October 2012)

Gold nanorods have been identified to be useful contrast agents as they exhibit pronounced two-photon photoluminescence under laser illumination of appropriate intensity and polarization configurations. In this paper, the two-photon photoluminescence imaging of three-dimensionally randomly oriented gold nanorods under linear and radial polarization illumination is investigated through a concentric energy analysis based on the Debye diffraction theory. Consequently, the effect of the numerical aperture and the apodization function of an objective on the polarization distribution in the focal region can be analyzed to form an important part in the understanding on the efficient excitation of gold nanorods. It is demonstrated that the radially polarized beam is an effective laser mode in generating strong two-photon imaging of nanorods in the presence of objectives with high numerical aperture and large annular obstruction sizes. © *2012 American Institute of Physics*. [http://dx.doi.org/10.1063/1.4759259]

I. INTRODUCTION

Gold nanoparticles are well known to generate strong two-photon photoluminescence (TPL) due to the enhanced surface plasmon resonance.[1] Distinct from other shaped gold nanoparticles, gold nanorods have a weak transverse and a strong longitudinal absorption bands, which correspond to the electron oscillation along the transverse and the longitudinal axes of a nanorod. Moreover, they possess a larger local field enhancement factor than other nanoparticles.[2] As a result, gold nanorods have been considered to be a promising contrast agent in a number of applications.[3–8] In particular, the unique size-dependent strong longitudinal absorption band is attractive in biomedical imaging, where the near-infrared (NIR) light source is used to minimize the scattering from skin and tissue.[4–7]

Intensive studies have been directed to the effect of the incident polarization direction on the excitation of a gold nanorod.[6–9] It has been revealed that the maximum excitation efficiency can be realized only when the incident polarization direction and the longitudinal axis of a nanorod are parallel with each other. As a result, a focal field of the x, y, and z components with the similar maximum intensity is preferred in gold nanorod enabled applications, where gold nanorods are three-dimensionally randomly oriented. It has been theoretically demonstrated that radially polarized beams are advantageous over linearly polarized beams when the polarization state in the focal region is manipulated.[10] Although strong TPL under radial polarization illumination has been experimentally observed for biological samples with a water-immersion objective in Ref. 7, only the polarization distribution in the focal region was investigated and no quantitative analysis of the orientations of the electromagnetic (EM) field vectors was undertaken. Furthermore, the influence of the orientations of the excited nanorods originating from the polarization distribution on the photoluminescence collection process, which is similar to the collection of fluorescence from dipoles, is yet revealed.

In addition to the effect of the polarization distribution the energy distribution in the focal region is an indispensable factor in the excitation of gold nanorods. The excitation efficiency of gold nanorods can be increased with the average power density (APD). However, the energy irradiance at the focal plane calculated based on the scalar diffraction theory[11,12] is insufficient to accurately evaluate the energy distribution in the presence of objectives with high numerical aperture (NA). Therefore, it is highly desirable to employ the vectorial Debye diffraction theory to investigate the energy distribution at the focal plane.[13]

In this paper, the vectorial Debye diffraction theory is adopted to calculate the concentric energy and the polarization distribution in the focal region of the high NA objectives. The method is used to analyze the TPL imaging of three-dimensionally randomly orientated gold nanorods for different values of the NA, the incident power and the apodization of objectives under linear and radial polarization illumination from both the excitation and the collection perspectives. Section II presents the definitions of the Debye-diffraction-based concentric energy and the polarization polar diagram. Sections III and IV are a comparative study on TPL imaging of gold nanorods in polyvinyl alcohol (PVA) under radial and linear polarization illumination. The analysis of the experimental results with a water-immersion objective (NA = 1.2) in Ref. 7 for practical applications is also carried out in Section V. A final finding of this study is given in Section VI.

[a)]Author to whom correspondence should be addressed. Electronic mail: mgu@swin.edu.au.

II. CONCENTRIC ENERGY ANALYSIS BASED ON THE DEBYE DIFFRACTION THEORY

The detail of the vectorial Debye diffraction theory has been well documented.[13,14] Based on this, we can calculate the vectorial light distributions in the focal region as well as the concentric energy.

For the investigation on the energy distribution at the focal plane, the total energy passing through the aperture is given by the aperture integral

$$F = \int_{\varepsilon}^{1} [T(r)]^2 2rdr, \tag{1}$$

where $T(r)$ is a transmission function of the aperture and ε is the size of the obstruction size for an annular aperture. Given the same amount of the incident energy at the focal plane, the total energy distributed over a given image radius r can be expressed by the image integral of the irradiance $I(r')$ over r', normalized by the factor F

$$Energy(r) = (1/F)\int_{0}^{r} I(r')2\pi r'dr'. \tag{2}$$

In order to quantitatively analyze the polarization distribution in the focal region, a newly defined approach with polar diagrams is employed. The orientation of this EM field vector projected on a given plane is determined by the angle between its direction and the $+x$ axis. The orientation range of 360° is split into 36 sections with each section having an angle range of 10°. The strength of the projected EM field vectors is hence included into a sole section according to its orientation rather than its spatial position in the plane. Thus, an equation is defined as follows:

$$Percentage = \frac{\sum_{i} |\boldsymbol{E}|}{\sum_{0^\circ}^{360^\circ} \sum_{i} |\boldsymbol{E}|}, \tag{3}$$

where $|\boldsymbol{E}|$ is the strength of the projected EM field vector and the index i ranging from 0 to 35 denotes a section in the plane. For a specific i, the top of Eq. (3) is the sum of the strength of the projected EM field vectors with the orientation represented by i and the bottom is the sum of the strength of the total EM field vectors projected in the plane.

III. EXPERIMENTAL SETUP AND SAMPLES

Gold nanorods, which had an average length of 45 nm and an average width of 11 nm with an overall concentration of 0.5×10^{-10} mol/L, were prepared using the seeded synthetic method.[15] They had a weak transverse absorption peak at wavelength 520 nm and a strong longitudinal absorption peak at wavelength 780 nm. Prior to applying gold nanorods in practical devices, solid matrices are considered as a necessary bridge to study the optical properties of gold nanorods. In our experiment, PVA served as a suitable matrix to accommodate gold nanorods because of the demonstrated stability under pulsed laser irradiation.[16,17] To avoid the aggregation, the gold nanorods were dispersed into a 10% PVA solution at a volume ratio of 1:1. The thickness of the gold nanorod doped PVA film was approximately 10 μm.

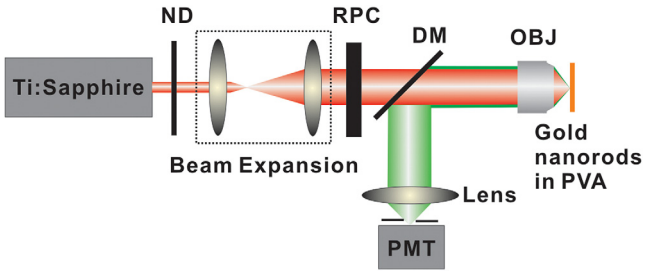

FIG. 1. Experimental setup for the TPL imaging of gold nanorods in PVA films. ND: neutral density filter; RPC: radial polarization converter; DM: dichroic mirror; OBJ: objective; PMT: photomultiplier tube.

Fig. 1 is the experimental setup for the TPL imaging of gold nanorod-PVA nanocomposite films. A linearly polarized femtosecond pulsed laser beam with a pulse width of 80 fs and a repetition rate of 80 MHz was generated by a Ti:Sapphire laser (Spectra-Physics: Mai-Tai). The linearly polarized beam was converted to a radially polarized beam by fulfilling the back aperture of a radial polarization converter (RPC) (Arcoptix S. A.) with a beam expansion system. The produced radially polarized beam consequently went through a focusing objective to excite the gold nanorods. The TPL generated by gold nanorods was collected by the same objective and separated from the excitation laser beam by a dichroic mirror before coupled to a photomultiplier tube (PMT). The incident power was controlled by a variable neutral density (ND) filter and measured in the focal spot. The good angular polarization uniformity of the converted radially polarized beam was demonstrated in Ref. 7.

IV. EFFECT OF AVERAGE POWER DENSITY AND POLARIZATION DISTRIBUTION

The effects of the APD and the polarization distribution in the focal region on the TPL of gold nanorods can be

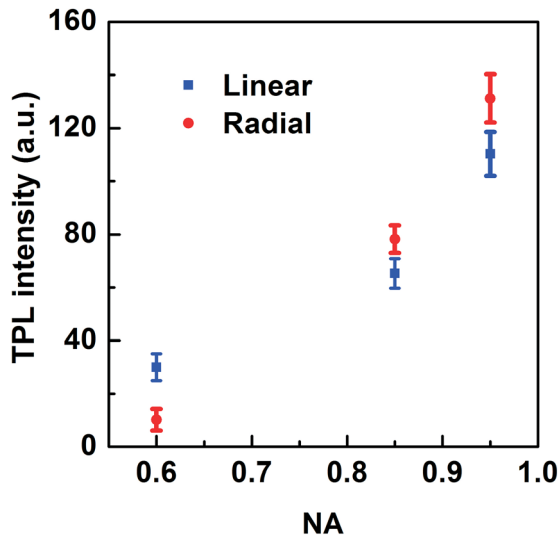

FIG. 2. Measured TPL intensity versus NA at 1.1 mW in the focal region under linear and radial polarization illumination.

investigated by the variation of the NA, the incident power, and the apodization of the objective.

A. Dependence of the two-photon photoluminescence imaging on numerical aperture

Fig. 2 shows the TPL imaging of gold nanorods at 1.1 mW in the focal region of objectives with different values of NA under linear and radial polarization illumination using the experimental setup shown in Fig. 1. The weaker TPL imaging was produced with the illumination of the radially polarized beam than that associated with the linear polarization illumination for NA = 0.6. However, the strong photoluminescence under radially polarized beam illumination was observed for objectives with NA = 0.85 and 0.95. Furthermore, the TPL intensity ratios between radial and linear polarization illumination rose from 1.15 to 1.35 when NA was increased from 0.85 to 0.95.

The calculated polar diagrams of the polarization distributions in the focal region of NA = 0.6, 0.85, and 0.95 under linear and radial polarization beam illumination are shown in Fig. 3. Assuming the incident linearly polarized beam is x polarized, it is obvious that the EM field vectors possess the main polarization direction along the x axis in the focal region for the three values of NA under linear polarization illumination. In contrast, the orientations of the EM field vectors projected in the x-y plane display a radial pattern with the radial polarization illumination regardless of NA. Moreover, the angle orientation ranges of the EM field vectors projected in the x-z (y-z) plane are wider than that under linear polarization illumination for these three objectives. For NA = 0.85 and 0.95, the longitudinal component becomes dominant in the focal region. These findings indicate that the more uniform polarization distributions are achieved under radial polarization illumination, which enhances the possibility of the efficient excitation of gold nanorods.

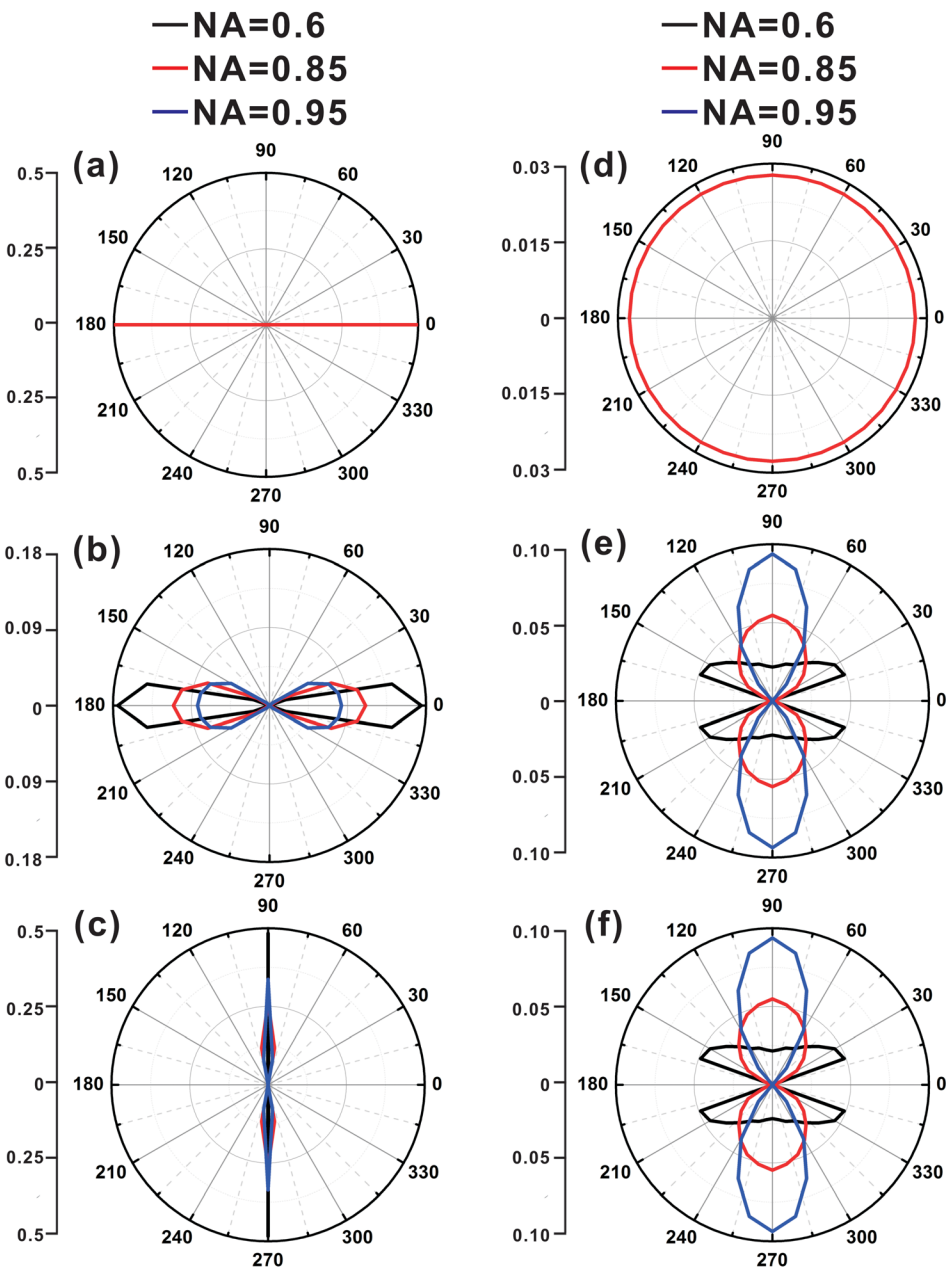

FIG. 3. Theoretical calculation on polar diagrams of the orientations of the EM field vectors in the focal region under linear (left) and radial (right) polarization illumination for NA = 0.6, 0.85, and 0.95 with $\varepsilon = 0$ in the focal volume. (a)-(c) and (d)-(f) are for the EM field vectors projected in the x-y, x-z, and y-z planes, respectively.

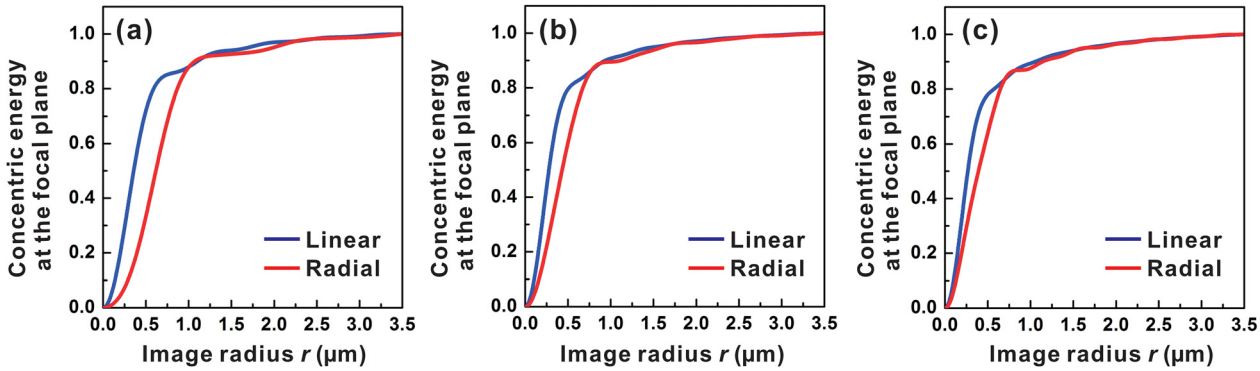

FIG. 4. Theoretical calculation on concentric energy as a function of image radius for objectives with NA = 0.6 (a), 0.85 (b), and 0.95 (c) under linear and radial polarization illumination.

Fig. 4 presents the dependences of the calculated concentric energy on the image radius at the focal plane under linear and radial polarization illumination for objectives with NA = 0.6, 0.85, and 0.95. The concentric energy and the corresponding APD in the image radius of a full width at the half maximum (FWHM) under both polarization illumination are summarized in Table I. The APD ratios between linear and radial polarization illumination for NA = 0.6, 0.85, and 0.95 are 3.35, 2.15, and 1.40, respectively, indicating that more energy is acting on the nanorods under linear polarization illumination but the difference of the energy effect on the excitation of gold nanorods between these two polarization illumination experiences a rapid decrease with the rising of NA.

Now let us turn to the collection of TPL. Assume that the nanorod emission process is similar to that of dipoles. For a dipole situated at the central position, the geometrical collection efficiency of the power emitted by the dipole is described as[18]

$$C_d = \frac{1}{8}\{4 - 3\cos\theta_{\max} - \cos^3\theta_{\max} + 3(\cos^3\theta_{\max} - \cos\theta_{\max})\cos^2\Theta\}, \quad (4)$$

where $\theta_{\max}$ is the maximum converging angle of an objective and Θ is the angle between the dipole orientation and the optical axis (the z axis). It is noted that the maximum collection efficiency is achieved at $\Theta = 90^\circ$, where the collection of the dipole oriented in the x-y plane occurs. Equation (4) can be employed to refer to the case of the dipole collection of a gold nanorod. The radiation emitted by a gold nanorod is symmetrically perpendicular to the dipole orientation. As the longitudinal absorption peak is much stronger than the transverse absorption peak, only the dipole excited by the longitudinal absorption band is considered. In this paper, an excited dipole from a gold nanorod with the longitudinal axis along the z direction is called a vertical dipole. For a gold nanorod with the longitudinal axis parallel to the x-y plane, the excited dipole is named a horizontal dipole.

TABLE I. Analysis of the calculated concentric energy (CE) and APD in the image radius of the FWHM at the focal plane as well as collection efficiency ratios between the vertical and the horizontal dipoles for objectives with NA = 0.6, 0.85, and 0.95 under linear and radial polarization illumination.

0.6				0.85				0.95			
Linear		Radial		Linear		Radial		Linear		Radial	
CE	APD	CE	APD	CE	APD	CE	APD	CE	APD	CE	APD
0.51	1.24	0.72	0.37	0.52	2.00	0.41	0.93	0.54	2.12	0.28	1.51
$C_{\text{vertical}}/C_{\text{horizontal}}$ 20.6%				$C_{\text{vertical}}/C_{\text{horizontal}}$ 49.6%				$C_{\text{vertical}}/C_{\text{horizontal}}$ 72.4%			

The collection efficiency ratios between the vertical and the horizontal dipoles ($C_{\text{vertical}}/C_{\text{horizontal}}$) for objectives with NA = 0.6, 0.85, and 0.95 under full aperture beam illumination ($\varepsilon = 0$) are also presented in Table I. It is revealed that the value of C_{vertical} is 20.6% of that of $C_{\text{horizontal}}$ for NA = 0.6, which demonstrates that the collection of the vertical dipoles is negligible compared with that of the horizontal dipoles. As shown in Fig. 3, the fact that the EM field vectors in the focal region are mainly polarized along the x direction under linear polarization illumination makes the collection of the photoluminescence mostly produced by the horizontal dipoles efficient due to the high value of $C_{\text{horizontal}}$. However, the negligible value of C_{vertical} is a disadvantage in collecting the total photoluminescence under radial polarization illumination because the longitudinal polarization component has the similar maximum strength as the transverse component. As a result, the combination of the low $\text{APD}_{\text{radial}}$ and the negligible C_{vertical} leads to the weak TPL imaging of gold nanorods under radial polarization illumination.

For NA = 0.85, the value of C_{vertical} is approximately 50% of that of $C_{\text{horizontal}}$, showing that the collection of the vertical dipoles cannot be ignored. When NA goes up to 0.95, the collection efficiency ratio between the vertical and the horizontal dipoles is further increased to 72.5%. The increased value of C_{vertical} enhances the collection efficiency of the vertical dipoles excited by the dominating longitudinal component in the case of radial polarization illumination. Given the conditions of the excitation of gold nanorods and the photoluminescence collection, we can make a conclusion that brighter TPL imaging should be produced under radial polarization beam illumination for NA = 0.85 and 0.95 owing to the more uniform polarization distribution in the focal region and the rising of C_{vertical} as well as the increased ratio between $\text{APD}_{\text{radial}}$ and $\text{APD}_{\text{linear}}$.

Compared with NA = 0.85, the collection of the vertical dipoles excited by the stronger dominating longitudinal component for NA = 0.95 under radial polarization illumination is facilitated by the higher collection efficiency ratio between the vertical and the horizontal dipoles. In addition, the high APD_{radial} enhances the excitation of gold nanorods for NA = 0.95. Thus, the ratio of the TPL intensity between radial and linear polarizations beam becomes larger when NA is increased from 0.85 to 0.95.

B. Dependence of the two-photon photoluminescence imaging on incident power

Fig. 5 presents the measured TPL intensity as a function of the incident power with an objective of NA = 0.85 under linear and radial polarization illumination. There are two common findings for both polarization illumination conditions: (1) the slopes of approximately 2 on the fitting lines demonstrate the two-photon excitation process for both polarization conditions and (2) stronger photoluminescence is observed with the increased power because the TPL intensity is proportional to $|E|^4$. A comparison of the TPL imaging under linear and radial polarization illumination can be determined by the intercept on the fitting lines. The intercept of 2.12 associated with radial polarization illumination is higher than 2.03 under linear polarization illumination, indicating that the bright TPL imaging is observed when the radially polarized beam is focused. One of the reasons for the generation of the stronger TPL imaging results from the more uniform polarization distribution in the focal region. Furthermore, the value of $C_{vertical}$, which is increased to 50% of that of $C_{horizontal}$, enhances the collection of the vertical dipole excited by the dominating longitudinal component. As a consequence, the use of radial polarization illumination is advantageous in producing bright TPL imaging for NA = 0.85.

C. Dependence of the two-photon photoluminescence imaging on annular beam illumination

Annular beam illumination is appealing not only in the improvement of the image resolution but also in the manipulation of the energy and polarization distributions in the focal region.[10,12,13,19,20] In this section, a thorough investigation on the relationships between TPL imaging and ε for low and high NA objectives is carried out.

Based on the previous experiments on the TPL imaging for NA = 0.6 under full aperture illumination ($\varepsilon = 0$), the dependences of the measured TPL intensity on ε under linear and radial polarization illumination are presented (Fig. 6). It can be seen that the TPL intensity remained almost unchanged for both polarization conditions when ε became larger.

According to Fig. 7, it is obvious that there is a small change in the orientations of the EM field vectors in the focal region with the rising of ε under both polarization conditions implying that the polarization uniformity cannot be greatly improved for the efficient excitation of gold nanorods.

From the dependence of the calculated concentric energy on the image radius at the focal plane (Fig. 8), the concentric energy and the APD in the image radius of the FWHM are shown in Table II. The APD_{linear} ratio and the APD_{radial} ratio between $\varepsilon = 0$, 0.36, and 0.7 are 1.94:1.55:1 and 1.42:1.41:1, respectively, which shows that the APD is decreased with the rising of ε for both polarization illumination and hence makes the excitation of gold nanorods less efficient from the point view of the energy effect.

In order to understand the photoluminescence collection, the collection efficiency ratios between the vertical and horizontal dipoles for NA = 0.6 with $\varepsilon = 0$, 0.36, and 0.7 are calculated (Table II). Although the ratio between $C_{vertical}$ and $C_{horizontal}$ is increased with the increased value of ε, it is only 30.8% for $\varepsilon = 0.7$ showing that the collection of the vertical dipoles is still too weak compared with that of the horizontal dipoles. Moreover, the approximately unchanged maximum

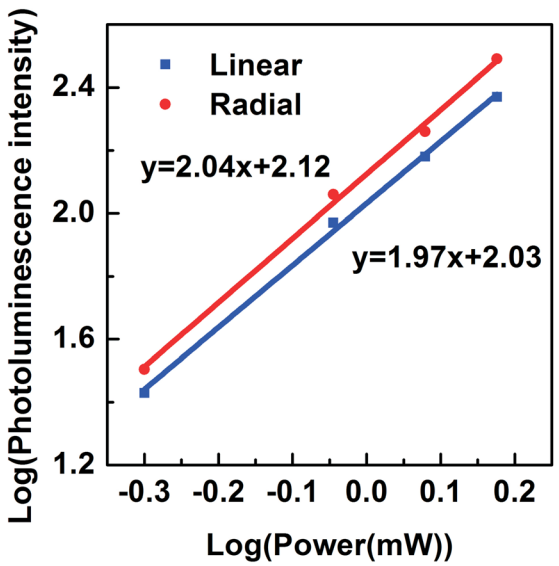

FIG. 5. Measured TPL intensity versus power on a logarithmic scale in the focal region of NA = 0.85 under linear and radial polarization illumination.

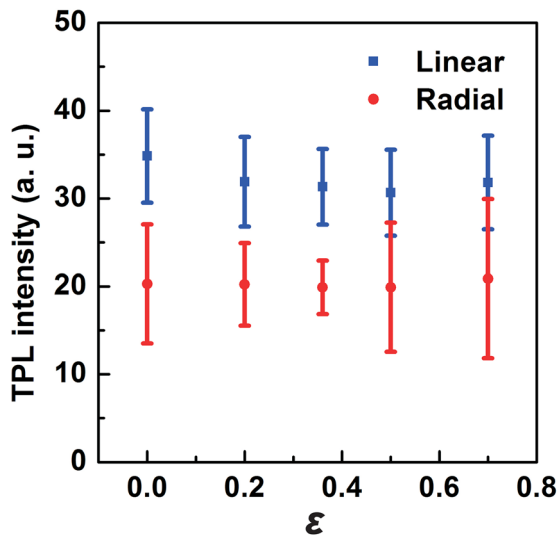

FIG. 6. Measured TPL intensity versus ε with NA = 0.6 under linear and radial polarization illumination.

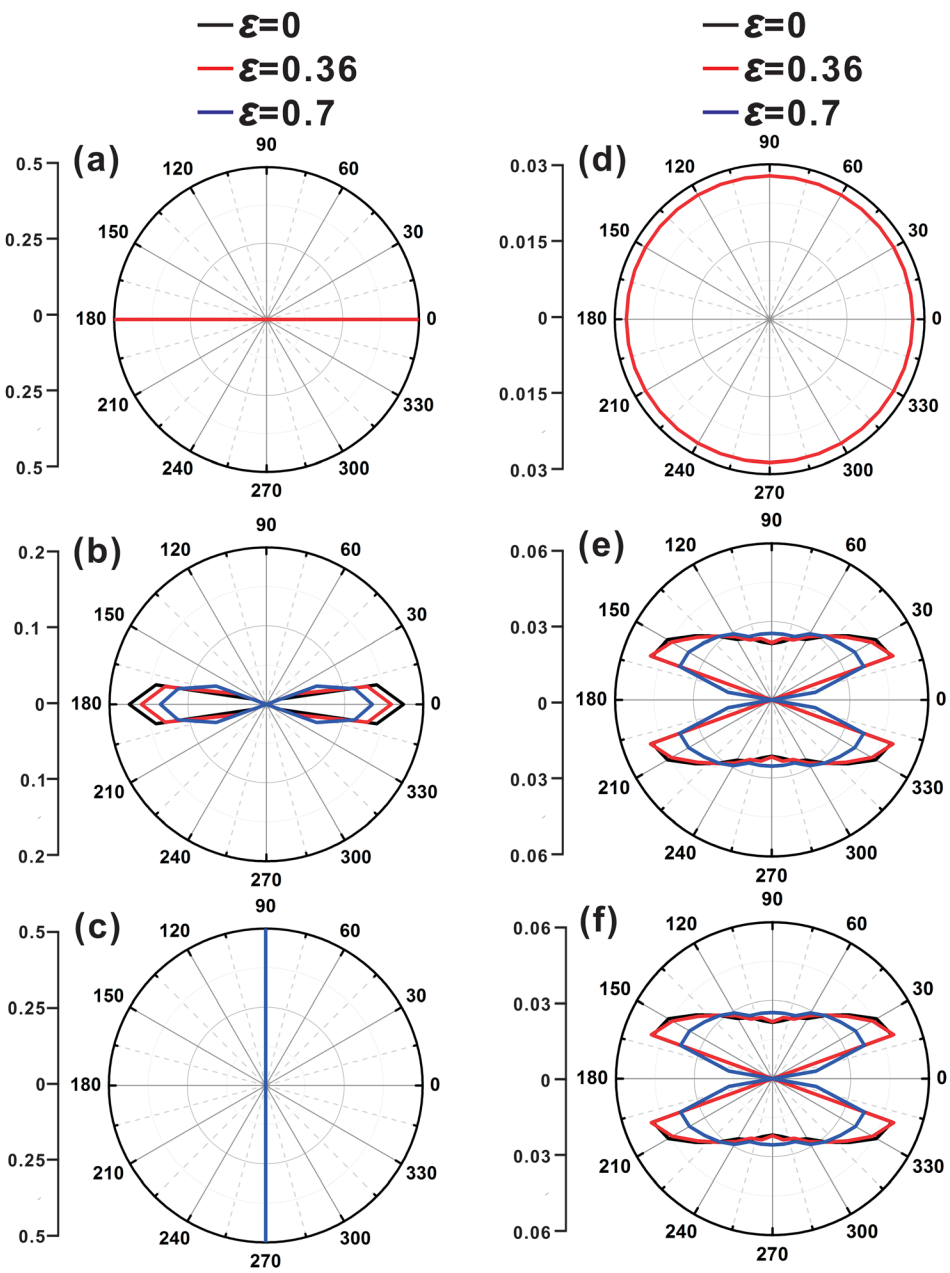

FIG. 7. Theoretical calculation on polar diagrams of the orientations of the EM field vectors in the focal region under linear (left) and radial (right) polarization illumination for NA = 0.6 with $\varepsilon = 0$, 0.36, and 0.7 in the focal volume. (a)-(c) and (d)-(f) are for the EM field vectors projected in the *x*-*y*, *x*-*z*, and *y*-*z* planes, respectively.

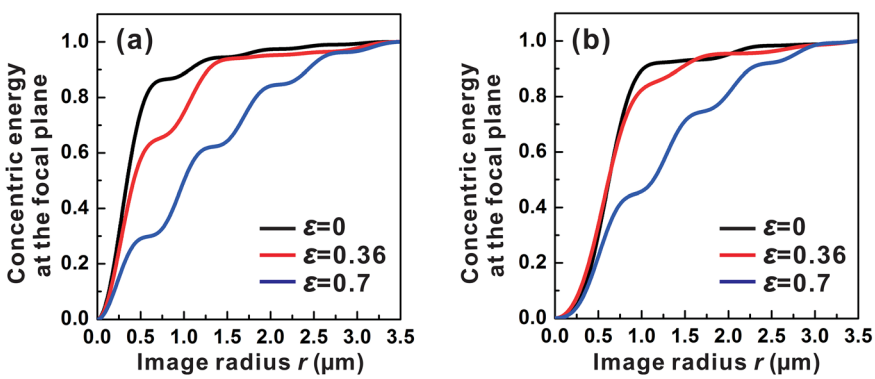

FIG. 8. Theoretical calculation on concentric energy as a function of image radius at the focal plane for a NA = 0.6 objective with $\varepsilon = 0$, 0.36, and 0.7 under linear (a) and radial (b) polarization beam illumination.

percentages of the longitudinal component for all the EM field vectors projected in the *x*-*z* plane under both linear and radial polarization illumination with the rising of ε indicate that the collection efficiency of the vertical dipoles can only be slightly improved with the moderate rising of C_{vertical}, thus making the total photoluminescence collection enhanced to a small extent. As a result, the decreased APD and the increased value of C_{vertical} result in the unvaried TPL intensity for NA = 0.6 with different values of ε under both polarization illumination.

TABLE II. Analysis of the calculated CE and APD in the image radius of the FWHM at the focal plane as well as collection efficiency ratios between the vertical and the horizontal dipoles for a NA = 0.6 objective with $\varepsilon = 0$, 0.36, and 0.7 under linear and radial polarization illumination.

0				0.36				0.7			
Linear		Radial		Linear		Radial		Linear		Radial	
CE	APD	CE	APD	CE	APD	CE	APD	CE	APD	CE	APD
0.51	1.24	0.72	0.37	0.45	0.99	0.66	0.37	0.19	0.64	0.34	0.26
$C_{vertical}/C_{horizontal}$ 20.6%				$C_{vertical}/C_{horizontal}$ 23.3%				$C_{vertical}/C_{horizontal}$ 30.8%			

Fig. 9 illustrates the dependence of the measured TPL intensity on ε at 1.1 mW in the focal region under linear and radial polarization illumination when NA was 0.85. The TPL intensity under linear polarization illumination was kept almost constant regardless of ε. In comparison with the low NA case, the TPL intensity exhibited a distinct dependence on ε under radial polarization illumination. A sharp rise started from $\varepsilon = 0.5$ and the TPL intensity for $\varepsilon = 0.75$ was increased to twice that for $\varepsilon = 0$. The analysis of the excitation and collection conditions is shown as follows.

The theoretical analysis on the polarization distributions in the focal region of NA = 0.85 for $\varepsilon = 0$, 0.5, and 0.75 illustrates that the dominant x component appears making the EM field vectors mainly parallel with the x direction under linear polarization illumination (Fig. 10). In comparison, under radial polarization illumination, the EM field vectors are preferably aligned at a small angle with respect to the z axis owing to the dominating longitudinal component and the angle orientation range becomes smaller with the larger value of ε.

The relationships between the calculated concentric energy and the image radius in the focal plane for NA = 0.85 with $\varepsilon = 0$, 0.5, and 0.75 under linear and radial polarization illumination are shown in Fig. 11 to study the energy effect

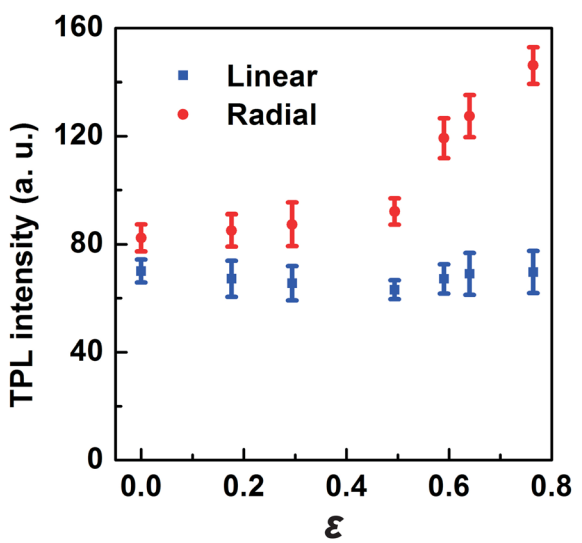

FIG. 9. Dependence of the measured TPL intensity on ε with NA of 0.85 at 1.1 mW in the focal region under linear and radial polarization illumination.

on the gold nanorod excitation. As the pronounced depolarization effect appears in the focal region for high NA objectives with large values of ε, the high side-lobes containing the high energy cannot be neglected. Therefore, the concentric energy and the APD in the image radii of the FWHM and 1.5 × FWHM are shown in Table III. In terms of linear polarization illumination, the APD_{linear} ratios between $\varepsilon = 0$, 0.5, and 0.75 in the image radii of the FWHM and 1.5 × FWHM are 1:0.69:0.37 and 1:0.67:0.36, respectively, indicating that the APD_{linear} in the image radii of either the FWHM or 1.5 × FWHM can be used to evaluate the energy fluence on the excitation of gold nanorods. It can be seen that the APD_{linear} is decreased with the rising of ε. The APD_{linear} for $\varepsilon = 0.7$ drops to 36% for $\varepsilon = 0$, which means that the efficiency of the energy interaction with gold nanorods is greatly reduced when ε becomes large. For radial polarization illumination, the APD_{radial} ratio between $\varepsilon = 0$, 0.5, and 0.75 in the image radius of the FWHM (1:1:0.79) is also approximately the same as that in the image radius of 1.5 × FWHM (1:1:0.77). No obvious change in the APD_{radial} is found for ε up to 0.5, achieving the same effect of the energy on the excitation of gold nanorods. When ε further increases to 0.75, the APD_{radial} is decreased by only 22% compared with that for $\varepsilon = 0$, which means that the interaction of the energy with gold nanorods becomes slightly inefficient.

According to the collection efficiency ratios between the vertical and the horizontal dipoles for NA = 0.85 with $\varepsilon = 0$, 0.5, and 0.75 (Table III), it is obvious that the value of $C_{vertical}$ is approaching the value of $C_{horizontal}$ with the rising of ε, realizing the efficient collection of the vertical dipoles. It is revealed that the maximum percentage of the longitudinal component for all sections of the EM field vectors projected in the x-z plane remains the same under linear polarization illumination, which indicates that the collection efficiency can be improved to a small extent with the increased value of $C_{vertical}$. Combined with the decreased APD_{linear}, we can make a conclusion that the TPL intensity stays the same independent of ε.

Compared with the case of $\varepsilon = 0$, the maximum percentages of the longitudinal component for all sections of the EM field vectors projected in the x-z (y-z) plane for $\varepsilon = 0.5$ under radial polarization illumination are increased by 20%. With the unchanged APD_{radial}, the high value of $C_{vertical}$ enables the vertical dipoles with the slightly increased strength to be more efficiently collected, resulting in a moderate increase in the TPL intensity. For $\varepsilon = 0.75$, the peak percentage of the longitudinal component for all sections of the EM field vectors projected in the x-z plan is 1.53 times that for $\varepsilon = 0$, which indicates that the dominating vertical dipoles can be remarkably collected by the increased value of $C_{vertical}$. As a consequence, despite the slightly decreased APD_{radial}, the TPL intensity for $\varepsilon = 0.75$ experiences a dramatic rise.

V. EFFECT OF A WATER-IMMERSION OBJECTIVE

Based on the above analysis of the TPL imaging of gold nanorods distributed in the PVA, the methods developed in the paper can be applied to understand the TPL

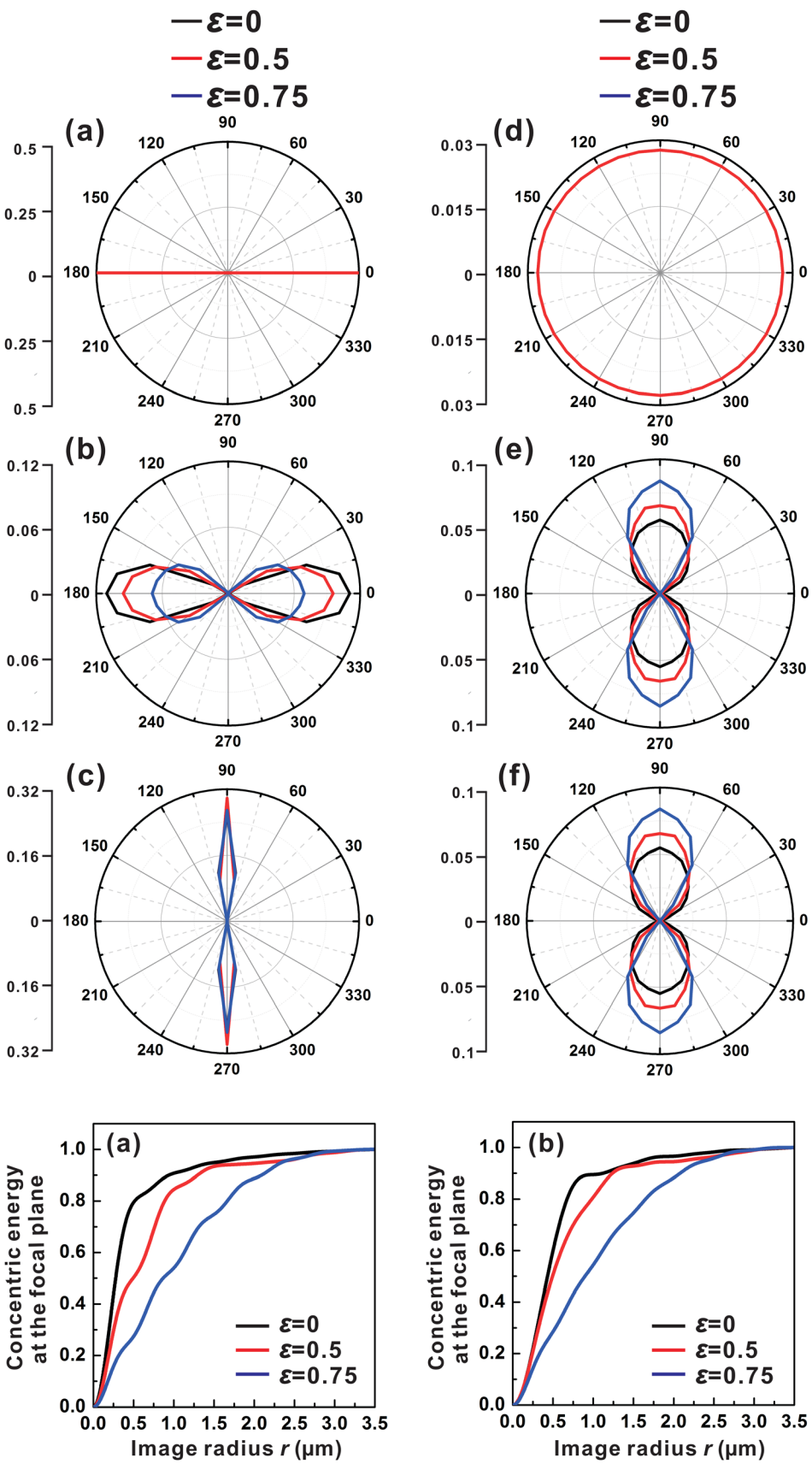

FIG. 10. Theoretical calculation on polar diagrams of the orientations of the EM field vectors in the focal region under linear (left) and radial (right) polarization illumination with NA = 0.85 and $\varepsilon = 0$, 0.5, and 0.75 in the focal volume. (a)-(c) and (d)-(f) are for the EM field vectors projected in the *x*-*y*, *x*-*z*, and *y*-*z* planes, respectively.

FIG. 11. Theoretical calculation on concentric energy as a function of image radius at the focal plane for a NA = 0.85 objective with $\varepsilon = 0$, 0.5, and 0.75 under linear (a) and radial (b) polarization beam illumination.

imaging of gold nanorods in practical applications, including the detection of cancer cells.[4–7] In particular, in Ref. 7, a water-immersion objective with NA = 1.2 is utilized to minimize the image aberration. For this case, the theoretical investigations on the effects of the polarization distribution in the focal region, the concentric energy, and the collection efficiency of dipoles with different orientations are undertaken as follows.

TABLE III. Analysis of the calculated CE and APD in the image radii of the FWHM and 1.5 × FWHM at the focal plane as well as collection efficiency ratios between the vertical and the horizontal dipoles for a NA = 0.85 objective with $\varepsilon = 0$, 0.5, and 0.75 under linear and radial polarization illumination.

	0				0.5				0.75			
	Linear		Radial		Linear		Radial		Linear		Radial	
Image radius (FWHM)	CE	APD	CE	APD	CE	APD	CE	APD	CE	APD	CE	APD
1	0.53	2.00	0.41	0.93	0.33	1.38	0.29	0.94	0.18	0.73	0.13	0.74
1.5	0.75	1.26	0.68	0.69	0.46	0.85	0.47	0.69	0.24	0.45	0.21	0.53
	$C_{vertical}/C_{horizontal}$ 49.4%				$C_{vertical}/C_{horizontal}$ 62.1%				$C_{vertical}/C_{horizontal}$ 81.3%			

Fig. 12 illustrates the quantitative analysis of EM field vectors projected in the *x*-*y*, *x*-*z*, and *y*-*z* planes in the focal region of a NA = 1.2 objective at a coverglass/water interface ($n_1/n_2 = 1.515/1.33$) under linear and radial polarization illumination, respectively. In terms of linear polarization beam illumination, it is clearly seen that most of the EM field vectors projected in the *x*-*y* plane are aligned with the *x* direction. The EM field vectors projected in the *x*-*z* plane are located with a maximum angle of 30° with respect to the *x* direction and a majority of the EM field vectors are projected parallel with the *z* axis in the *y*-*z* plane. These polar diagrams show the *x* component is much stronger than the *y* and *z* components. On the contrary, for radial polarization illumination, the EM field vectors projected in the *x*-*y* plane are uniformly distributed in a radial pattern. The EM field vectors projected in the *x*-*z* and *y*-*z* planes are confined within a

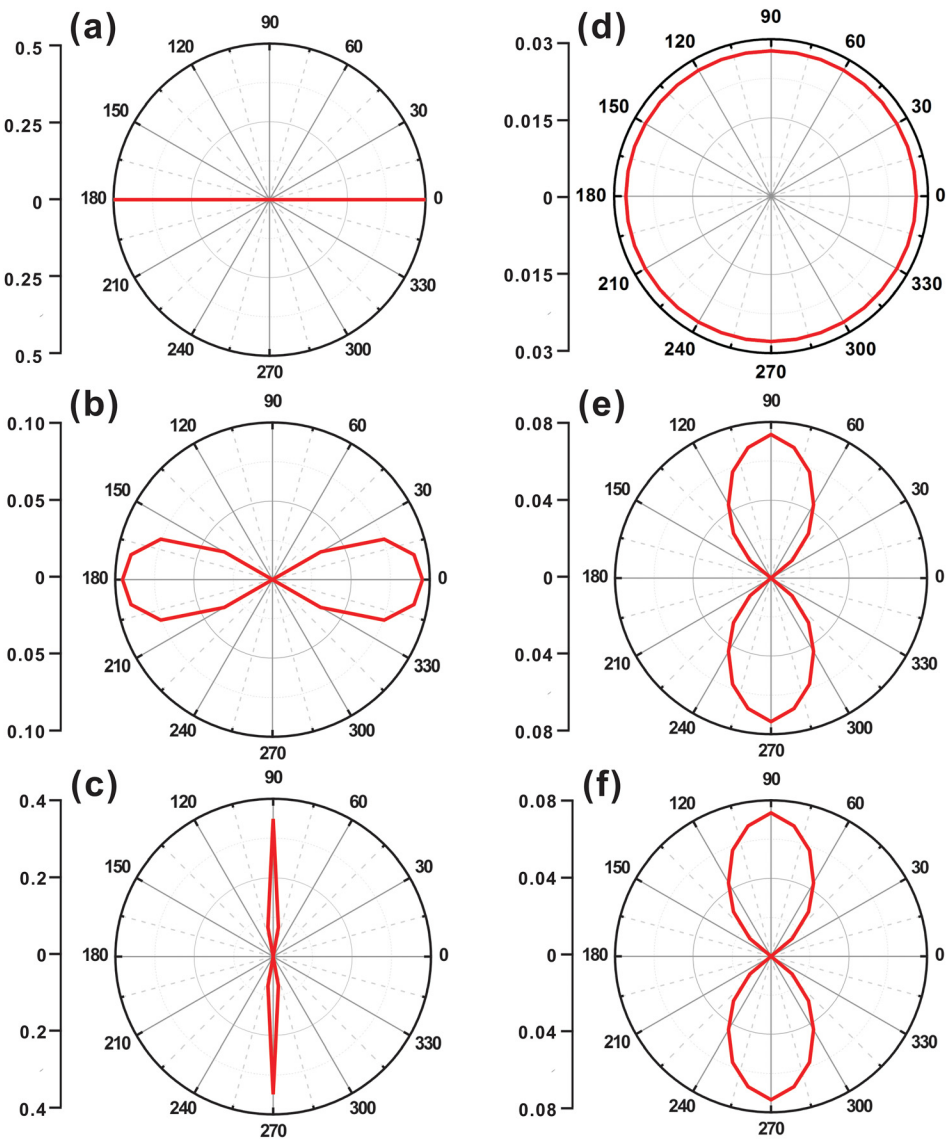

FIG. 12. Theoretical calculation on polar diagrams of the orientations of the EM field vectors in the focal region with a NA = 1.2 objective at a coverglass/water interface ($n_1/n_2 = 1.515/1.33$) under linear (left) and radial (right) polarization illumination. (a)-(c) and (d)-(f) are for the EM field vectors projected in the *x*-*y*, *x*-*z*, and *y*-*z* planes, respectively.

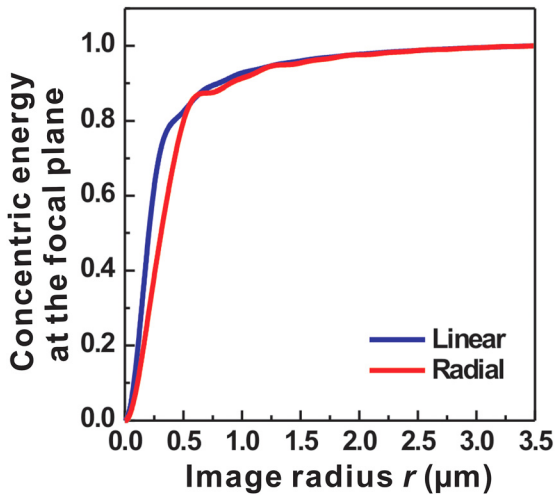

FIG. 13. Theoretical calculation on concentric energy as a function of image radius at the focal plane for a NA = 1.2 objective at a coverglass/water interface ($n_1/n_2 = 1.515/1.33$) under linear and radial polarization beam illumination.

maximum angle orientation of 30° with respect to the z axis, which indicates the longitudinal component is dominating in the focal region. Given the enhanced strength of the y and z polarization components compared to those produced under linear polarization illumination, it is expected that a radially polarized beam is advantageous in generating strong TPL imaging from the point view of the polarization distribution.

The energy effect on the TPL imaging is studied by calculating the concentric energy as a function of the image radius under linear and radial polarization illumination (Fig. 13). Considering the appearance of strong side-lobes with high energy in the presence of high NA, both the corresponding concentric energy and the APD in the image radii of the FWHM and 1.5 × FWHM are summarized in Table IV to investigate the energy distribution. It can be seen that the APD_{radial} is approximately 58% of the APD_{linear} in the image radius of the FWHM and is increased to 69% of the APD_{linear} when the image radius is expanded to 1.5 × FWHM. This finding indicates that the difference of the energy effects between linear and radial polarization illumination becomes smaller with the rising of the image radius.

From Table IV, it can be seen that the collection efficiency ratio of the vertical dipole to the horizontal dipole achieves 60% denoting that the horizontal dipoles excited by the dominating x component associated with linear polarization illumination can be efficiently collected and the low value of $C_{vertical}$ is a hurdle for the efficient collection of the dipoles by the dominant longitudinal component generated under radial polarization illumination. However, the more uniform polarization distribution associated with radial polarization illumination plays a major role in the enhancement of the excitation of the gold nanorods and hence the stronger TPL imaging was observed compared with linear polarization illumination.[7]

TABLE IV. Analysis of the calculated CE and APD in the image radii of the FWHM and 1.5 × FWHM at the focal plane as well as collection efficiency ratios between the vertical and the horizontal dipoles for a NA = 1.2 objective at a coverglass/water interface ($n_1/n_2 = 1.515/1.33$) under linear and radial polarization illumination.

	Linear		Radial	
Image radius (FWHM)	CE	APD	CE	APD
1	0.53	3.65	0.33	2.13
1.5	0.74	2.26	0.54	1.55
	$C_{vertical}/C_{horizontal}$			
	60%			

VI. CONCLUSION

In conclusion, the concentric energy analysis based on the Debye diffraction theory has been demonstrated to be a useful tool to understand the TPL images from three-dimensionally oriented gold nanorods. Our investigation into the effect of the NA, the incident power, and ε has been thoroughly studied under linear and radial polarization illumination, which revealed that concentric energy is essential to evaluate the light interaction with nanorods. A radially polarized beam has shown its capability of generating strong TPL imaging for objectives with high NA and large values of ε, which is promising in tight-focusing applications. It has been demonstrated that the TPL intensity under radial polarization illumination can be enhanced to be approximately twice that under linear polarization illumination for NA = 0.85 with ε = 0.75. The methodology developed in the paper has also been applied to further understand the TPL imaging and photothermal therapy in biological applications.

ACKNOWLEDGMENTS

The authors thank Dr. Baohua Jia and Dr. Hongchun Bao for their help discussions.

[1]G. T. Boyd, Z. H. Yu, and Y. R. Shen, Phys. Rev. B **33**, 7923 (1986).
[2]C. Sönnichsen, T. Franzl, T. Wilk, G. von Plessen, J. Feldmann, O. Wilson, and P. Mulvaney, Phys. Rev. Lett. **88**, 077402 (2002).
[3]P. Zijlstra, J. W. M. Chon, and M. Gu, Nature **459**, 410 (2009).
[4]X. Huang, I. H. El-Sayed, W. Qian, and M. A. El-Sayed, J. Am. Chem. Soc. **128**, 2115 (2006).
[5]L. Tong, Y. Zhao, T. B. Huff, M. N. Hansen, A. Wei, and J.-X. Cheng, Adv. Mater. **19**, 3136 (2007).
[6]J. Li, D. Day, and M. Gu, Adv. Mater. **20**, 3866 (2008).
[7]H. Kang, B. Jia, J. Li, D. Morrish, and M. Gu, Appl. Phys. Lett. **96**, 063702 (2010).
[8]X. Li, T. Lan, C. Tien, and M. Gu, Nat. Commun. **3**, 998 (2012).
[9]H. Wang, T. B. Huff, D. A. Zweifel, W. He, P. S. Low, A. Wei, and J.-X. Cheng, Proc. Natl. Acad. Sci. U.S.A. **102**, 15752 (2005).
[10]H. Kang, B. Jia, and M. Gu, Opt. Express **18**, 10813 (2010).
[11]G. C. Steward, *The Symmetrical Optical System* (The University Press, Cambridge, 1928).
[12]H. F. A. Tschunko, Appl. Opt. **13**, 1820 (1974).
[13]M. Gu, *Advanced Optical Imaging Theory* (Springer, Heidelberg, 2000).
[14]P. Török, P. Varga, Z. Laczik, and G. R. Booker, J. Opt. Soc. Am. A **12**, 325 (1995).
[15]T. K. Sau and C. J. Murphy, Langmuir **20**, 6414 (2004).
[16]Y. Dirix, C. Bastiaansen, W. Caseri, and P. Smith, Adv. Mater. **11**, 223 (1999).
[17]J. Pérez-Juste, B. Rodríguez-González, P. Mulvaney, and L. M. Liz-Marzán, Adv. Funct. Mater. **15**, 1065 (2005).
[18]T. Plakhotnik, W. E. Moerner, V. Palm, and U. P. Wild, Opt. Commun. **114**, 83 (1995).
[19]M. Gu, T. Tannous, and C. J. R. Sheppard, Opt. Commun. **110**, 533 (1994).
[20]C. J. R. Sheppard and A. Choudhury, Appl. Opt. **43**, 4322 (2004).